Check for updates

The preparation of a novel iron/manganese binary oxide for the efficient removal of hexavalent chromium [Cr(VI)] from aqueous solutions

Chuanxi Yang, [ID] [ab] Tiantian Ju,[c] Xiaoning Wang,[d] Yujia Ji,[e] Cheng Yang,[f] Haojie Lv,[a] Ying Wang,[a] Wenping Dong,[g] Feng Dang,[h] Xifeng Shi,[i] Weiliang Wang [ID] *[aj] and Yuqi Fan [ID] *[a]

To remove hexavalent chromium Cr(VI) efficiently, a novel Fe–Mn binary oxide adsorbent was prepared *via* a "two-step method" combined with a co-precipitation method and hydrothermal method. The as-prepared Fe–Mn binary oxide absorbent was characterized *via* transmission electron microscopy (TEM), scanning electron microscopy (SEM), X-ray diffraction (XRD), Fourier-transform infrared spectra (FTIR), thermogravimetric analysis (TGA), zeta potential, BET and X-ray photoelectron spectroscopy (XPS). The results indicated that the morphology of the adsorbent was rod-like with length of about 100 nm and width of about 50–60 nm, specific surface area was 63.297 m^2 g^{-1}, has the composition of α-Fe_2O_3, β-MnO_2 and $MnFe_2O_4$ and isoelectric point was observed at pH value of 4.81. The removal of Cr(VI) was chosen as a model reaction to evaluate the adsorption capacity of the Fe–Mn binary oxide adsorbent, indicating that the Fe–Mn binary oxide adsorbent showed high adsorption performance (removal rate = 99%) and excellent adsorption stability (removal rate > 90% after six rounds of adsorption). The adsorption behavior of the Fe–Mn binary oxide was better represented by the Freundlich model (adsorption isotherm) and the pseudo-second-order model (adsorption kinetic), suggesting that the adsorption process was multi-molecular layer chemical adsorption. The possible adsorption mechanism of the Fe–Mn binary oxide for the removal of Cr(VI) included the protonation process and the electrostatic attraction interactions.

1. Introduction

Chromium (Cr), especially hexavalent chromium Cr(VI), is widely found in natural environment (water, soil, and air).[1] Cr(VI) is introduced mainly from industrial processes, taking into account electroplating, tannery facilities, and chromium mining.[2,3] Due to the highly toxic and environmentally harmful nature of Cr(VI), it is essential to remove Cr(VI) from the environment.[4,5]

The removal of Cr(VI) from aqueous solutions has been extensively researched in the reference.[6] The common methods for the removal of Cr(VI) from aqueous solutions includes chemical redox,[7] precipitation,[8] ion exchange,[9] membrane separation,[10] and adsorption.[11,12] Among these methods (physical method, chemical method and biological method), the adsorption method has been agreed to be at the frontline for the removal of Cr(VI) from waste water due to its outstanding advantages such as easy to handle, highly selective, economically efficient and environmental friendly.[13–16]

The reported adsorbents for Cr(VI) removal includes carbon materials (activated carbons, coconut husk carbon), transition metal oxides (Fe_3O_4, MnO_2, Al_2O_3, TiO_2), and high-molecular polymer.[17–19] Due to the strong affinity between chromium and iron, and excellent magnetic property of the iron-based material, different types of iron-based materials have been studied and used as adsorbents for removal of Cr(VI).[20–23] For example, Hu and co-workers reported an effective adsorbent of jacobsite ($MnFe_2O_4$) to remove Cr(VI) from wastewater.[24] In fact, a Fe–Mn binary oxide may contain strong oxidation property

[a]Institute of Environment and Ecology, Shandong Normal University, Jinan 250358, China. E-mail: sdqcsdnu@163.com; yuqifan@sdnu.edu.cn; Fax: +86-531-8618-2550

[b]College of Resources and Environmental Sciences, China Agricultural University, Beijing 100193, China

[c]Construction Project Environmental Assessment Service Center of Shandong Province, Jinan 250012, China

[d]School of Mechanical Engineering and Automation, Northeastern University, Shenyang 110819, China

[e]College of Art and Science, University of Vermont, Burlington, VT 05405, USA

[f]School of Physics and Electronics, Shandong Normal University, Jinan 250014, China

[g]Shandong Academy of Environmental Science Co., Ltd., Jinan 250013, China

[h]Key Laboratory for Liquid-Solid Structural Evolution and Processing of Materials, Shandong University, Jinan 250061, China

[i]College of Chemistry, Chemical Engineering and Materials Science, Shandong Normal University, Jinan 250014, China

[j]College of Geography and Environment, Shandong Normal University, Jinan 250358, China

(manganese dioxide), high adsorption property (iron oxides), and excellent separating property (magnetic materials).[25–27] Hence, it is necessary to prepare an adsorbent with high adsorption capacity and propose the possible adsorption mechanism *via* characterization, adsorption performance, adsorption isotherm and adsorption kinetics.[28–32]

Herein, a novel Fe–Mn binary oxide adsorbent was prepared *via* a "two-step method" combined with the co-precipitation method and hydrothermal method, and the adsorbent was characterized by transmission electron microscopy (TEM), scanning electron microscopy (SEM), X-ray diffraction (XRD), Fourier-transform infrared spectra (FTIR), thermogravimetric analysis (TGA), zeta potential, BET and X-ray photoelectron spectroscopy (XPS). The removal of CrO_4^{2-} was chosen as a model reaction to evaluate the adsorption capacity of Fe–Mn binary oxide adsorbent. The results indicated that the Fe–Mn binary oxide adsorbent showed high adsorption performance and excellent adsorption stability. The adsorption behavior of Fe–Mn binary oxide was better represented by the Freundlich model (adsorption isotherm) and the pseudo-second-order model (adsorption kinetic). The possible adsorption mechanism of Fe–Mn binary oxide for the removal of Cr(vi) included the protonation process and the electrostatic attraction interaction.

2. Materials and methods

2.1 Materials

Potassium permanganate ($KMnO_4$), ferrous sulfate ($FeSO_4 \cdot 7H_2O$), sodium hydroxide (NaOH), ethyl alcohol (C_2H_5OH), hydrochloric acid (HCl), sulfuric acid (H_2SO_4), phosphoric acid (H_3PO_4), ammonium chloride (NH_4Cl), acetone (CH_3COCH_3) and diphenylcarbazide ($C_{13}H_{14}N_4O$) were purchased from Sinopharm Chemical Reagent Co., Ltd. Potassium chromate (K_2CrO_4) was purchased from Tianjin Guangcheng Chemical Reagent Co., Ltd. All these reagents were of AR grades and used without further purification. Deionized water was used for the preparation of all the solutions.

2.2 Adsorbent preparation

The novel Fe–Mn binary oxide adsorbent was prepared *via* a "two-step method" combined with the co-precipitation method and hydrothermal method. The typical synthesis of Fe–Mn binary oxide was described in Scheme 1. First, an appropriate amount of $KMnO_4$ and $FeSO_4 \cdot 7H_2O$ was dissolved in the deionized water, and these solutions were ultrasonicated for 30 min to ensure uniform mixing. The $KMnO_4$ solution was transferred to a 250 mL round-bottom flask, and the $FeSO_4 \cdot 7H_2O$ solution was transferred to a 100 mL constant pressure funnel. Then, the $FeSO_4 \cdot 7H_2O$ solution was added dropwise at the rate of 1 drop per second with stirring to obtain a red turbid liquid, and the pH value of the preparation was changed to 3 by adding 1 mol L^{-1} HCl during the co-precipitation process. Then, the above red turbid liquid was transferred to a 100 mL reaction still, and the reaction was continued for 6 h at 180 °C. The products were filtered and washed with deionized water, and the final products were kept for aging for 4 h at room temperature. Finally, the Fe–Mn binary oxide was obtained after freeze drying at 60 °C.

2.3 Adsorbent characterization

Transmission electron microscopy (TEM) pattern was performed on a JEM-1011 transmission electron microscope and was used to determine the grain sizes of the Fe–Mn binary oxide adsorbent.

Scanning electron microscopy (SEM) image with Energy Dispersive Spectrometer (EDS) was obtained on a QUANTA Q400 thermal-field emission scanning electron microscope and it was used to determine the morphology and aggregation status of the Fe–Mn binary oxide adsorbent.

X-ray diffraction (XRD) patterns were recorded on a Bruker D8 Advance X-ray diffractometer with Cu Kα radiation ($\lambda = 1.5418$ Å) and it was used to determine the crystal structure and phase composition of the Fe–Mn binary oxide adsorbent.

Fourier-transform infrared spectra (FT-IR) analysis was recorded on a Vertex 70 spectrometer in range of 4000 to 400 cm^{-1} and it was used to determine the functional groups and the composition of the Fe–Mn binary oxide adsorbent.

Thermogravimetric analysis (TGA) was performed with a Q500 thermal analysis instrument with heating from 30 to 800 °C at 10 °C min^{-1} both in air and N_2, and the results were used to determine the thermostability of the Fe–Mn binary oxide adsorbent.

Zeta potential was measured by a Malvern Zetasizer 2000 and it was used to determine the isoelectric point of the Fe–Mn binary oxide adsorbent.
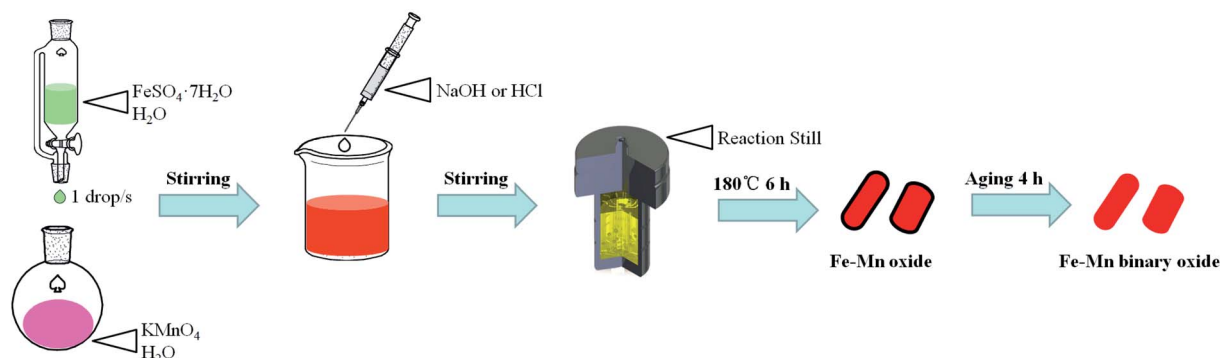
Scheme 1 Preparation of the Fe–Mn binary oxide adsorbent.

The surface texture of Fe–Mn binary oxide adsorbent was examined by the N_2 adsorption at 77 K (Quantachrome instruments Quadrasorb SI). The specific surface area was calculated from the N_2 adsorption isotherm using the BET equation.

X-ray photoelectron spectroscopy (XPS) measurements were performed on a Thermo ESCALAB 250Xi system with an Al Kα X-ray source. All of the binding energies were referenced to the C 1s peak at 284.8 eV for the surface adventitious carbon.

2.4 Batch adsorption tests

The stock solution containing 100 mg L^{-1} of Cr(VI) was prepared by dissolving 0.2828 g of K_2CrO_4 in 1000 mL of deionized water. Simulated wastewaters with different Cr(VI) concentration (5–100 mg L^{-1}) were prepared by the dilution of the stock K_2CrO_4 standard solution with deionized water. All the experiments were carried out in a 100 mL beaker containing 50 mL of simulated wastewater at 25 °C. The initial pH of Cr(VI) solution was 6.4 without pH adjustment. In some cases, the initial pH values of the Cr(VI) solution were adjusted to 2 and 12 by the addition of 0.1 mol L^{-1} H_2SO_4 and 0.1 mol L^{-1} NaOH, respectively. The pH values were measured with an Orion model 920A pH/ISE meter with a Beckman combination electrode. Batch removal studies were carried out at the desired contact time and adsorbent dosage levels, where the concentrations of Fe–Mn binary oxide adsorbent ranged from 1 to 5 g L^{-1}. After the adsorption process, the samples were analyzed by the diphenylcarbazide spectrophotometry with TU-1900 double beam UV-visible light spectrophotometer at maximum absorption wavelength λ_{max} = 540 nm. The removal rate (R) of Cr(VI) and the amount of Cr(VI) adsorbed per unit mass of the adsorbent (q_e) were evaluated by using the mass balance equations as follow:[33,34]

$$R = (c_0 - c_e)/c_0 \times 100\%$$

$$q_e = V(c_0 - c_e)/W$$

where R (%) is the removal rate of Cr(VI), c_0 (mg L^{-1}) is the initial concentration of Cr(VI), c_e (mg L^{-1}) is the equilibrium concentration of Cr(VI), q_e (mg g^{-1}) is the mean adsorbing capacity, V

(L) is the volume of the solution, and W (g) is the mass of the adsorbent.

3. Results and discussion

3.1 Characterization of Fe–Mn binary oxide adsorbent

3.1.1 TEM and SEM. The TEM image of the Fe–Mn binary oxide adsorbent was clearly displayed in Fig. 1a. It can be confirmed that the morphology of the adsorbent is rod-like nanocomposite with length about 100 nm and width about 50–60 nm. Meanwhile, the nano-decussation was generated by the aggregation of the Fe–Mn binary oxide adsorbent, which was caused by the enough magnetism and high surface energy of the Fe–Mn binary oxide nanorod.[35] SEM and EDS are the prominent characterization methods for studying the morphology and elemental composition of the Fe–Mn binary oxide adsorbent. The SEM image Fig. 1b demonstrated the aggregation phenomenon of the Fe–Mn binary oxide, and the aggregate was composed of a uniform rod-like nanocomposite, similar to the TEM results. The EDS analysis (Table 1) revealed that the Fe/Mn molar ratio was about 2.71, which was approaching to the initial $FeSO_4 \cdot 7H_2O$/$KMnO_4$ molar ratio (value = 3) and XPS result (value = 3.25).

3.1.2 XRD and FT-IR. The XRD pattern in Fig. 2a of the Fe–Mn binary oxide adsorbent matched well with the α-Fe_2O_3

Table 1 EDS and XPS results of Fe–Mn binary oxide adsorbent

Characterization	Element	Content	Fe/Mn molar ratio
EDS	Fe	34.08[a] wt%	2.71
	Mn	12.36 wt%	
	C	43.25 wt%	
	O	10.31 wt%	
XPS	Fe	20.88[b] at%	3.25
	Mn	6.42 at%	
	C	19.38 at%	
	O	53.33 at%	

[a] wt% represents the percentage of weight. [b] at% represents the percentage of atom.
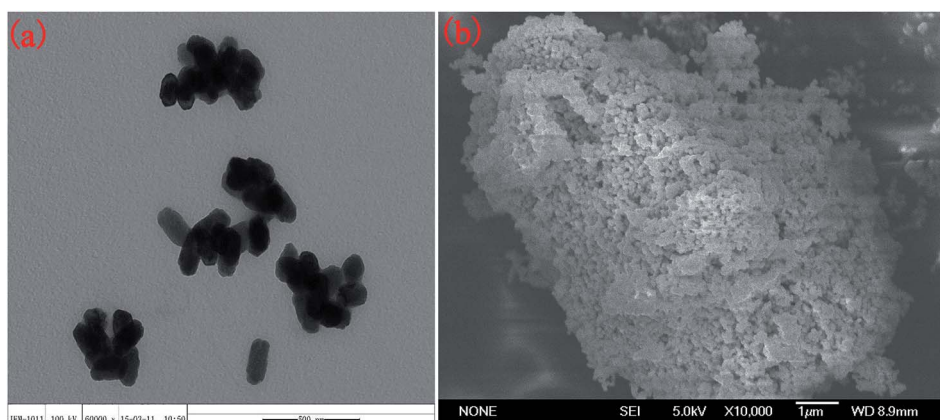

Fig. 1 TEM image (a) and SEM image (b) of Fe–Mn binary oxide adsorbent.
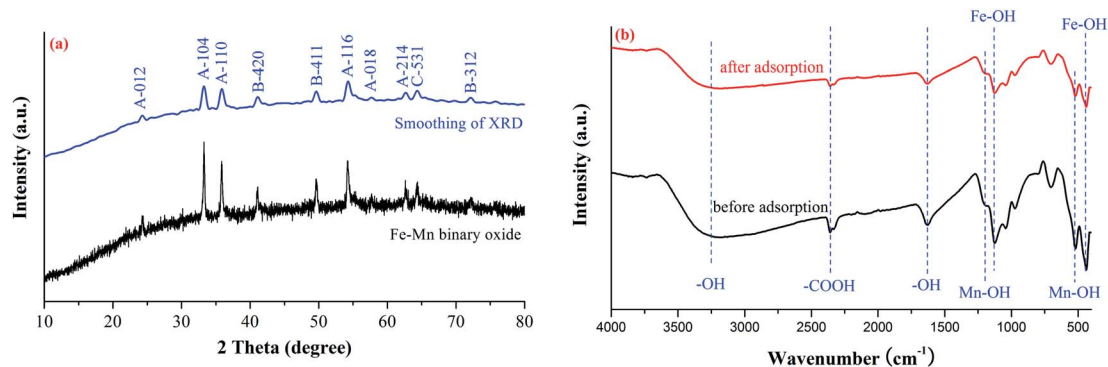
Fig. 2 XRD pattern (a) and FT-IR spectrum (b) of Fe–Mn binary oxide adsorbent.

(JCPDS card file 33-0664, $a = b = 5.036$ Å, $c = 13.749$ Å, space group $R\bar{3}c$[167]), β-MnO$_2$ (JCPDS card file 44-0141, $a = b = 9.785$ Å, $c = 2.863$ Å, space group $I4/m$[87]) and MnFe$_2$O$_4$ (JCPDS card file 10-0319, $a = b = 8.499$ Å, $c = 8.499$ Å, space group $Fd\bar{3}m$ [227]). The diffraction peaks at $2\theta = 24.138°$, $33.152°$, $35.611°$, $54.089°$, $57.589°$ and $62.449°$, corresponded to the reflections from the (012), (104), (110), (116), (018) and (214) planes of hematite α-Fe$_2$O$_3$, respectively. The diffraction peaks at $2\theta = 41.225°$, $49.864°$ and $72.711°$, corresponded to the reflections from the (420), (411) and (312) planes of manganese oxide β-MnO$_2$, respectively. The diffraction peak at $2\theta = 64.798°$, corresponded to the reflections from the (531) planes of jacobsite MnFe$_2$O$_4$, respectively.[36]

The FTIR spectrum of the Fe–Mn binary oxide adsorbent was shown in Fig. 2b. The main characteristic bands of Fe–Mn binary oxide were assigned as follows:[37,38] the intensive peaks at 3228 cm^{-1} and 1627 cm^{-1} can be attributed to the –OH stretching vibration band from H$_2$O and Fe(OH)$_3$. The characteristic peaks at 1123 cm^{-1} and 435 cm^{-1} are associated with Fe–OH (Fe$_2$O$_3$) and goethite α-FeOOH stretching vibration bands. Meanwhile, the characteristic peaks at 1202 cm^{-1} and 515 cm^{-1} are associated with Mn–OH and β-MnO$_2$ stretching vibration bands. In addition, the peak at 2359 cm^{-1} is associated with the oxygen-containing functional group (such as

–COOH) stretching vibration on the surface of Fe–Mn binary oxide adsorbent.

3.1.3 Zeta potential. A plot of zeta potential of Fe–Mn binary oxide *versus* pH (2.0–12.0) was shown in Fig. 3a. It should be noted that the zeta potential *versus* pH curve was positive at low pH (<4) and negative at high pH (>6). The zeta potential of Fe–Mn binary oxide decreased with increase in pH. At low pH, the zeta potential reached the higher value due to the increased potential of H$^+$ ions in solution. However, in alkaline solution, the zeta potential adopted negative values due to the increased potential of OH$^-$ ions in solution. The isoelectric point has been observed at pH value of 4.81 in Fig. 3b.

3.1.4 BET. It is well-known that the BET surface area of a sample is an essential parameter for an enhanced adsorption activity. The adsorption and desorption isotherms of N$_2$ at 77 K on Fe–Mn binary oxide adsorbent are shown in Fig. 4a. The results indicated that the prepared adsorbent was a Type II isotherm characteristic mesoporous material, which was in agreement with the pore diameter as shown in Fig. 4b. The Fe–Mn binary oxide adsorbent has a specific surface area of 63.297 m^2 g^{-1} based on the BET test, which is 1/2 times of the Fe–Mn based adsorbent prepared by Malgorzata Szlachta and co-author, however, the adsorption capacity of Fe–Mn binary oxide in this work was 3/4 times of the Fe–Mn binary oxide
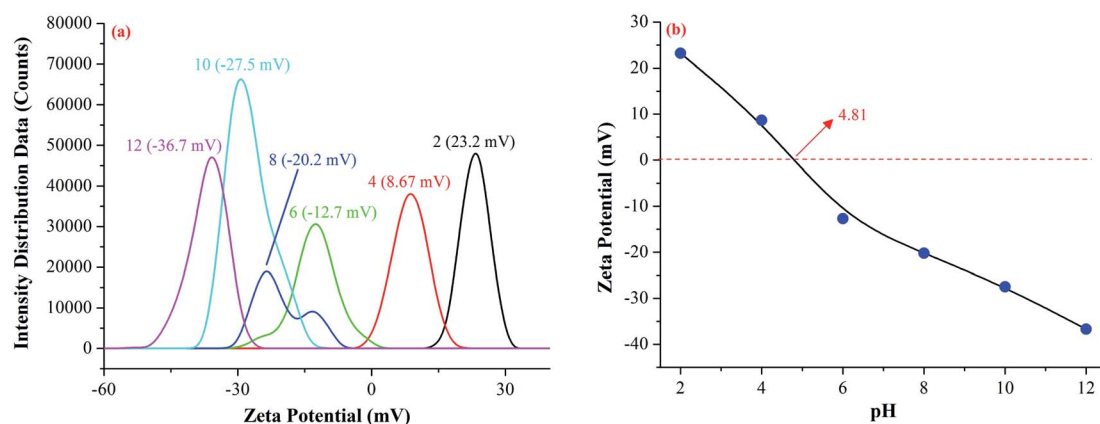

Fig. 3 Zeta-potential in solutions of various pH with 2, 4, 6, 8, 10 and 12 (a) and the variation curve of zeta potential as a function of pH value (b) for Fe–Mn binary oxide adsorbent.
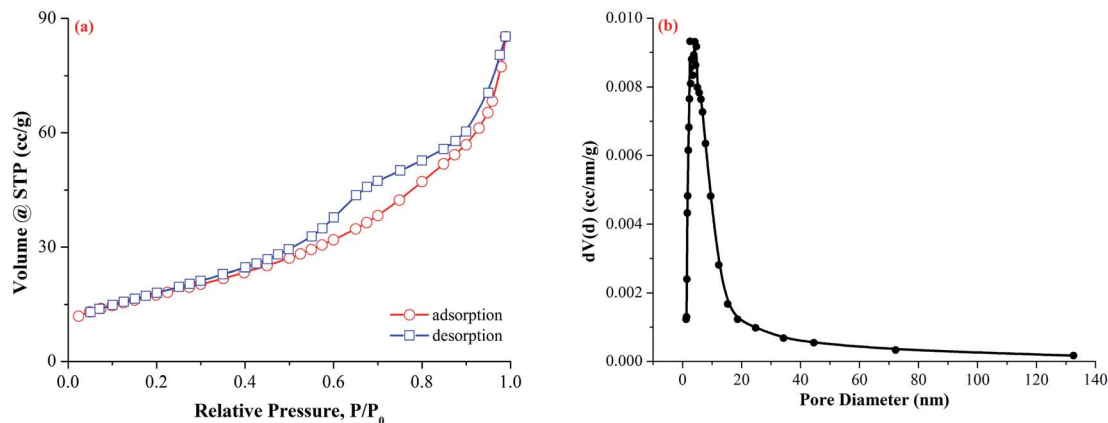
Fig. 4 N$_2$ adsorption and desorption isotherms at 77 K (a) and pore diameter (b) of Fe−Mn binary oxide adsorbent.

prepared by Malgorzata Szlachta and co-author.[39] The results indicated that the surface area of an adsorbent is only an index to character the physicochemical properties, not the decisive index to ensure the adsorption capacity.

3.1.5 XPS. XPS was used to examine the oxidation states of the iron and manganese in the Fe–Mn binary oxide system. The XPS spectra of Fe 2p, Mn 2p, O 1s and C 1s on Fe–Mn binary oxide adsorbent were shown in Fig. 5a and Table 1. The atomic percentages of Fe, Mn, O and C were 20.88%, 6.42%, 53.33% and 19.38%, respectively. The Fe/Mn molar ratio was about 3.25, which approached to the initial $FeSO_4 \cdot 7H_2O$/KMnO$_4$ molar ratio (value = 3) and EDS result (value = 2.71). The results of Fe 2p and Mn 2p electron binding energies are shown in Fig. 5b and c. The Fe 2p$_{1/2}$ and Fe 2p$_{2/3}$ peak positions (724.8 eV and 711.1 eV) and shape are characteristic of Fe(III). The Mn 2p$_{1/2}$ and Mn 2p$_{3/2}$ peaks at 654.5 and 642.8 eV with a spin energy separation of 11.7 eV was assigned to be the 2p binding energy of Mn(IV) and it matched well with the characteristic peaks of MnO$_2$. Meanwhile, the Mn 2p$_{1/2}$ and Mn 2p$_{3/2}$ peaks at 653.9 and 642.2 eV with a spin energy separation of 11.7 eV was assigned to be the 2p binding energy of Mn(II) and matches well with the characteristic peaks of jacobsite MnFe$_2$O$_4$.[40,41] The broad peak of O 1s can be fitted by two peaks at binding energies of 530.0 eV and 531.4 eV in Fig. 5d. The dominant peak at 530.0 eV is characteristic of oxygen in metal oxide (O^{2-}), and a shoulder peak at around 531.4 eV suggests the presence of –OH oxygen (Fe–OH and Mn–OH) on the surface of Fe–Mn binary oxide adsorbent. Meanwhile, the peak of C 1s can be fitted by three peaks at binding energies of 284.8 eV, 286.4 eV and 288.6 eV in Fig. 5e, corresponding to C–C/C=C, C=O and O–C=O bonds on the surface of the Fe–Mn binary oxide adsorbent, respectively.[42]

3.2 Adsorption capacity of Fe–Mn binary oxide adsorbent

Adsorption activity tests were investigated by the removal of CrO_4^{2-} in aqueous solution. The samples were analyzed by the diphenylcarbazide spectrophotometry with TU-1900 double beam UV-visible light spectrophotometer at maximum absorption wavelength λ_{max} = 540 nm. Fig. 6a shows the removal of CrO_4^{2-} in the presence of the Fe–Mn binary oxide adsorbent

prepared with different molar ratios between Fe and Mn. As can be seen, the adsorbing capacity of the absorbent and the removal rate of Cr(VI) showed increasing–decreasing trend with the molar ratio between Fe and Mn being increased, and the optimum molar ratio between Fe and Mn was 3 : 1. It was well-known that the adsorption property of the Fe–Mn binary oxide depended on the particle size and specific surface area of the absorbent, and particle size and specific surface area were influenced by the initial molar ratio between Fe and Mn during the preparation process. When the initial molar ratio between Fe and Mn was low (<3 : 1), with the increase in the molar ratio between Fe and Mn, the Fe^{3+} was hydrolyzed to Fe(OH)$_3$ and this reaction was good for increasing the specific surface area of the absorbent. However, when the molar ratio between Fe and Mn continued to increase (>3 : 1), the superfluous Fe^{3+} and Mn^{4+} were separated from the aqueous solution as precipitates and this precipitation was bad for the removal of Cr(VI).[43]

The adsorption property of the Fe–Mn binary oxide for the removal of Cr(VI) was measured and the influence of the adsorbent dosage, pH value and initial concentration of Cr(VI) solution was studied, and the results were shown as Fig. 6b, c and d, respectively.

The effect of the adsorbent dosage on the adsorption of Cr(VI) was shown in Fig. 6b with initial molar ratio between Fe and Mn = 3 : 1, pH value = 3, and initial concentration of Cr(VI) = 100 mg L^{-1}. It was obvious, that the removal rate of Cr(VI) increased from 60% to 93% with absorbent dosage increased from 0.05 g to 0.25 g, but the adsorbing capacity was decreased from 61 mg g^{-1} to 19 mg g^{-1}. The adsorption property with different adsorbent dosage was influenced by the adsorption sites. When the adsorbent dosage was low (0.05 g), with the adsorbent dosage increasing, absorbent provided more adsorption sites, which was good for increasing the removal rate of Cr(VI). However, when the adsorbent dosage continued to increase (0.15 g), the adsorption sites were enough and the limiting factor was the concentration of Cr(VI), therefore the removal rate of Cr(VI) was almost unchanged but the adsorbing capacity was decreased.[44]

The effect of pH value on adsorption of Cr(VI) was shown in Fig. 6c, with initial molar ratio between Fe and Mn = 3 : 1,
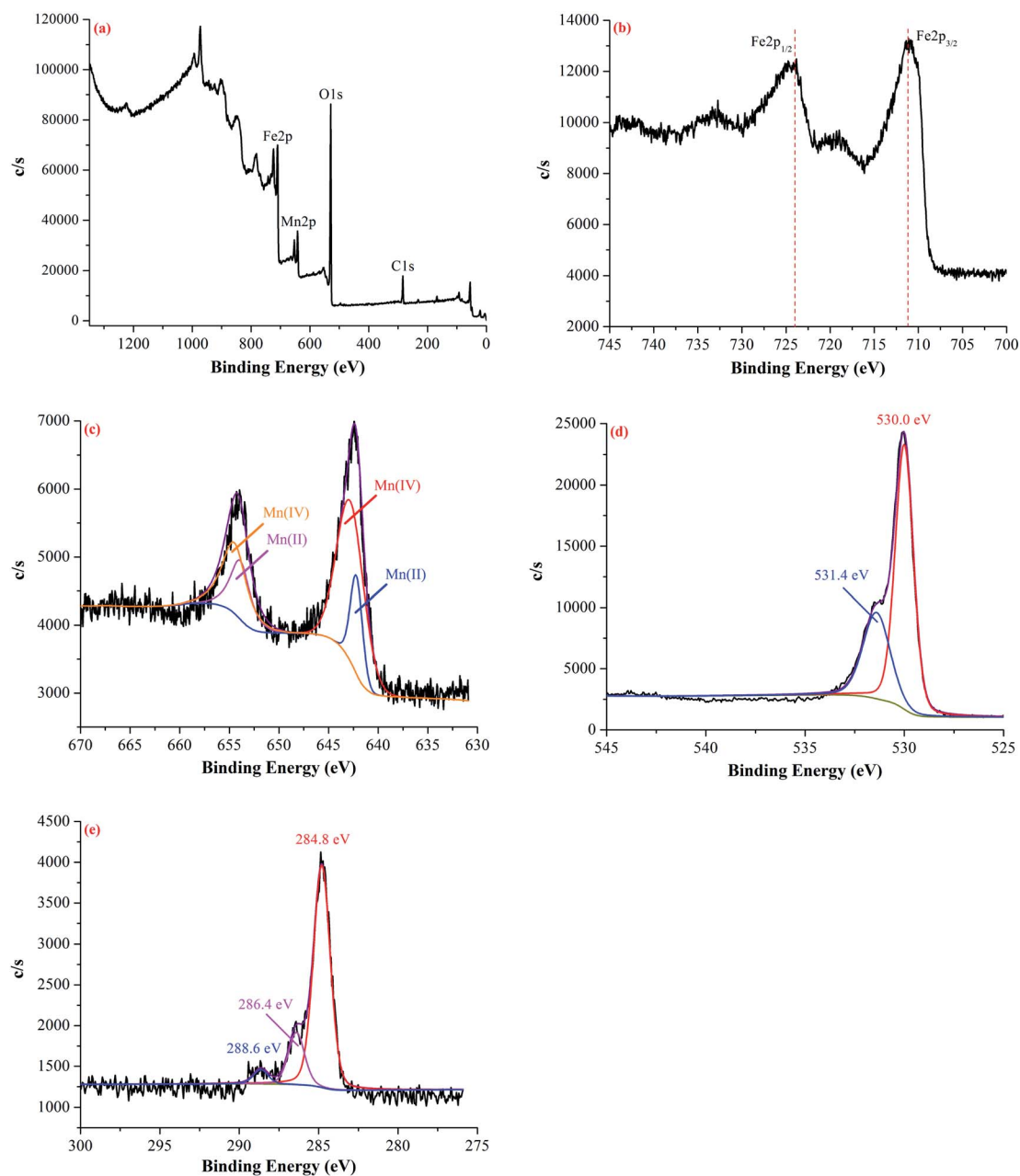
Fig. 5 XPS spectra (a), high-resolution spectra of Fe 2p (b), Mn 2p (c), O 1s (d) and C 1s (e) of Fe−Mn binary oxide adsorbent.

adsorbent dosage = 0.15 g, and initial concentration of Cr(VI) = 100 mg L^{-1}. It was obvious that the removal rate of Cr(VI) decreased from 93% to 50% and the adsorbing capacity was decreased from 31 mg g^{-1} to 17 mg g^{-1}, with pH value increased from 2 to 12. The adsorption property with different pH value was influenced by the electrostatic adsorption. When the pH value < 7, the absorbent was protonated with positive charges on the surface, and the pH value was lowered, the positive charges were more, the electrostatic adsorption was stronger, which is good for the removal of Cr(VI). When the pH value > 7, the absorbent was deprotonated with negative charges on the surface, and the pH value was higher, the negative charges were more, the electrostatic repulsion was stronger, which is bad for the removal of Cr(VI).[45]

The effect of initial concentration of Cr(VI) on the adsorption of Cr(VI) was shown in Fig. 6d, with initial molar ratio between Fe and Mn = 3 : 1, adsorbent dosage = 0.15 g, and pH value = 3. It was obvious that the adsorbing capacity was increased from 3 mg g^{-1} to 31 mg g^{-1} with initial concentration of Cr(VI) being increased from 5 mg L^{-1} to 100 mg L^{-1}, but the removal rate of Cr(VI) increased from 91% (5 mg L^{-1}) to 99% (20 mg L^{-1}) and decreased from 99% (20 mg L^{-1}) to 93% (100 mg L^{-1}). The adsorption property with different initial concentration of Cr(VI) was influenced by the adsorption sites. When the initial concentration of Cr(VI) was increased from 20 mg L^{-1}, the
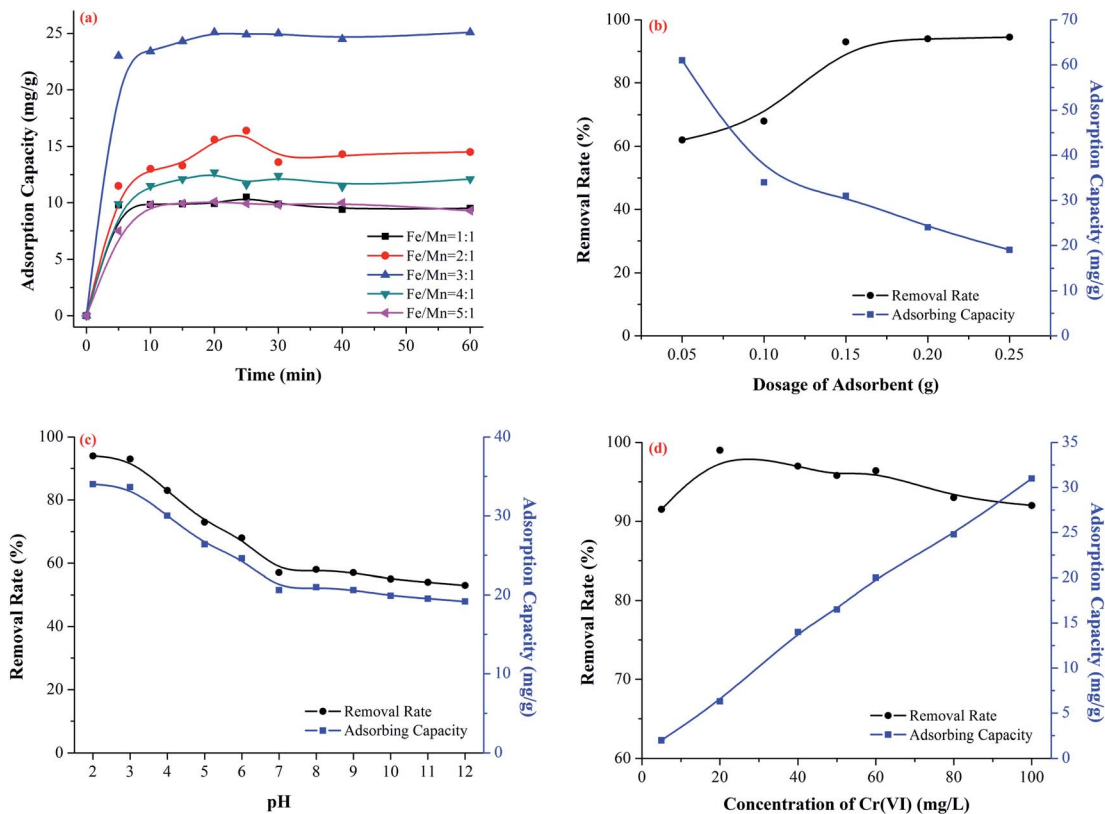
Fig. 6 Effects of molar ratio between Fe and Mn (a), adsorbent dosage (b), pH value (c) and initial concentration of Cr(VI) (d) on adsorption of Cr(VI).

removal rate of Cr(VI) decreased from 99% to 93% and the adsorbing capacity was increased from 7 mg g^{-1} to 31 mg g^{-1} due to the limited adsorption sites. However, when the initial concentration of Cr(VI) was excessively low (5 mg L^{-1}), it was unexpected that the removal rate of Cr(VI) was 91%, which was lower than that of 20 mg L^{-1} (99%), this phenomenon was due to the reason that the adsorption sites were superfluous without being fully utilized.[46]

3.3 Adsorption mechanism of Fe–Mn binary oxide adsorbent

The adsorption isotherm of Cr(VI) on Fe–Mn binary oxide adsorbent was treated with various initial Cr(VI) concentrations (5–100 mg L^{-1}) at 25 °C (Fig. 7a). Two adsorption isotherms, namely, Langmuir model (Fig. 7c) and Freundlich model (Fig. 7d), were used to analyze the adsorption behavior. The adsorption kinetics describing the removal rate of Cr(VI) on Fe–Mn binary oxide adsorbent was one of the important characteristics that define the efficiency of removal (Fig. 7b). The pseudo-first-order model (Fig. 7e) and pseudo-second-order model (Fig. 7f) models were used to interpret the adsorption behavior.[47,48]

3.3.1 Adsorption isotherms. Equilibrium adsorption isotherm tests were performed by transferring 0.15 g absorbent and 50 mL Cr(VI) solution (5–100 mg L^{-1}) to a capped tube prior to shaking in a temperature-controlled orbital shaker (200 rpm). Experiments were performed at 25 ± 1 °C and at pH value = 3.

The Langmuir model (E1) and Freundlich model (E2) equations were used to estimate the isotherm parameters for Cr(VI) adsorption onto Fe–Mn binary oxide absorbent:[49–51]

$$\frac{c_e}{q_e} = \frac{1}{q_m}c_e + \frac{1}{q_m b} \tag{E1}$$

$$\lg q_e = \lg k + \frac{1}{n}\lg c_e \tag{E2}$$

where q_e (mg g^{-1}) is the equilibrium adsorption capacity; q_m is the maximum monolayer adsorption capacity (mg g^{-1}); c_e (mg L^{-1}) is the equilibrium concentration of Cr(VI); b (L mg^{-1}) is the Langmuir adsorption equilibrium constant that is related to the binding energy; k (mg g^{-1}) (L mg^{-1}) is the Freundlich constant that is related to the adsorption capacity; and n is the adsorption intensity parameter.

The results from the Cr(VI) adsorption equilibrium experiments on the Fe–Mn binary oxide absorbent were shown in Fig. 7c and d, respectively. The adsorption constants obtained from the isotherms were listed in Table 2.

As shown in Fig. 7c and d and Table 2, high regression coefficients ($R^2 > 0.95$) suggested that both Langmuir model and Freundlich model adsorption isotherm were suitable for describing the adsorption behavior of Cr(VI) by Fe–Mn binary oxide absorbent. However, the regression coefficients in Table 2 indicated that the Freundlich model fitted better than the Langmuir model, suggesting that the adsorption process was
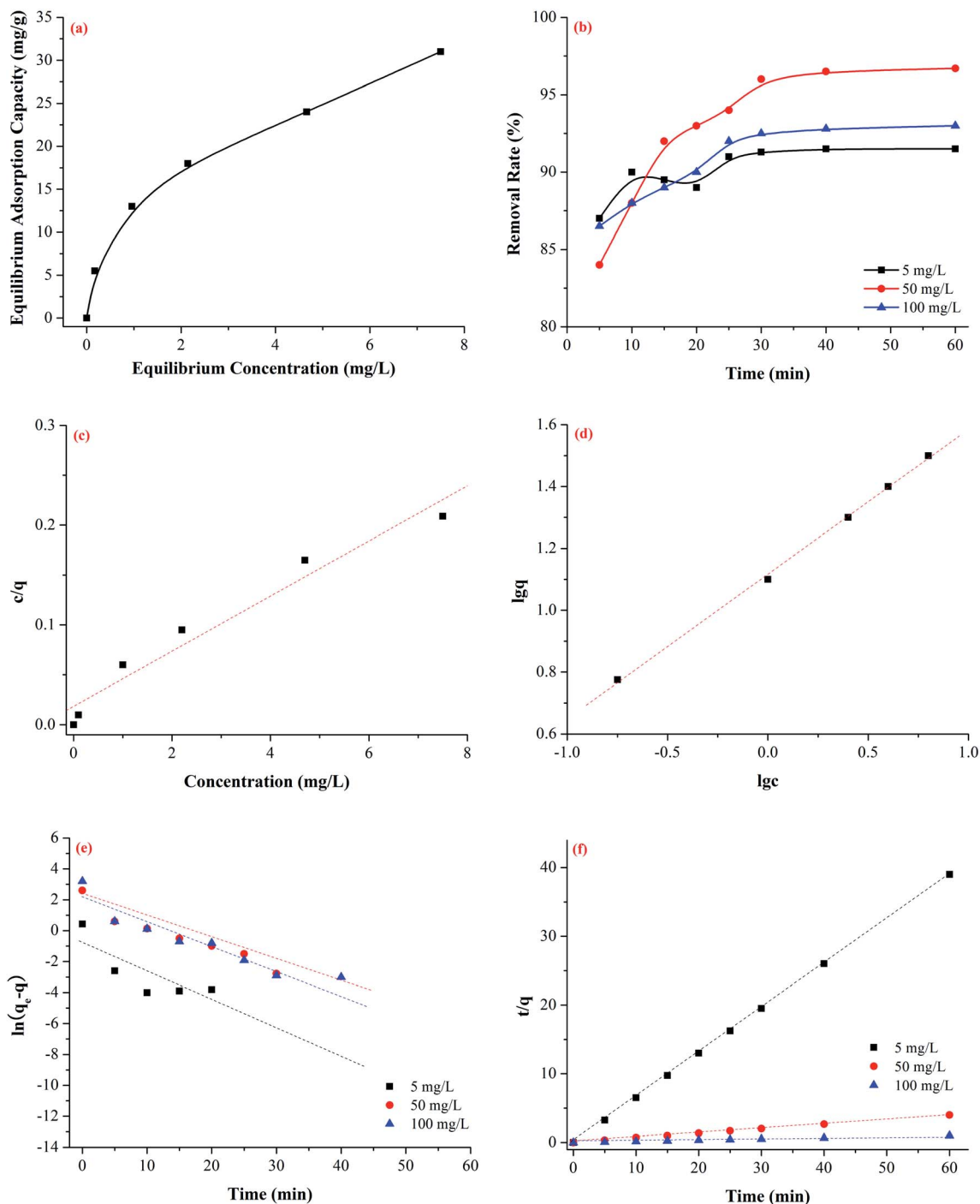
Fig. 7 Adsorption isotherm (a) and adsorption kinetic (b) of Fe−Mn binary oxide adsorbent with different initial concentration of Cr(VI), Langmuir model (c) and Freundlich model (d) of adsorption isotherm, and pseudo-first-order model (e) and pseudo-second-order model (f) of adsorption kinetic.

non-ideal adsorption (multi-molecular layer adsorption) and the surface of Fe–Mn binary oxide is relatively heterogeneous. Meanwhile, the value of $1/n$ was less than 0.5, indicating that the adsorption process is favorable.[52,53]

3.3.2 Adsorption kinetics. Adsorption kinetic experiments were performed at different Cr(VI) concentrations (5, 50 and 100 mg L^{-1}) for 1 h, at absorbent dosage = 0.15 g, temperature = 25 ± 1 °C and pH value = 3. Kinetic tests were carried out

using a magnetic stirrer (IKA, Germany) set at 200 rpm. To determine the constant temperature for Cr(VI) adsorption, a temperature-controlled water bath was used.

To investigate the adsorption kinetics of Cr(VI) on Fe–Mn binary oxide adsorbent, two models were used to describe the adsorption behavior. The classical model included the pseudo-first-order equation (E3) and the pseudo-second-order model (E4).[54,55]

Table 2 Langmuir model and Freundlich model adsorption isotherm parameters for Cr(VI) adsorption on Fe−Mn based absorbent at temperature = 25 ± 1 °C and pH = 3

Model	Parameter	Value
Langmuir model	$q_m{}^a$ (mg g^{-1})	32.26
	$q_m*{}^b$ (mg g^{-1})	30.83
	b (L mg^{-1})	1.148
	R^2	0.9581
Freundlich model	k ((mg g^{-1}) (L mg^{-1}))	13.52
	$1/n$	0.4077
	R^2	0.9986

^{a} The maximum adsorption capacity on Langmuir model adsorption isotherm. ^{b} The maximum adsorption capacity on adsorption test.
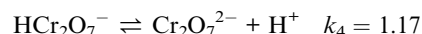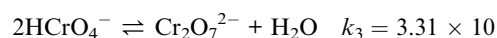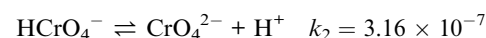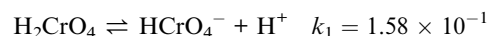
$$\ln(q_e - q) = \ln q_e - k_1 t \qquad (E3)$$

$$\frac{t}{q} = \frac{1}{k_2 \times q_e^2} + \frac{1}{q_e} t \qquad (E4)$$

where q (mg g^{-1}) is adsorption capacity at time t; q_e (mg g^{-1}) is the equilibrium adsorption capacity; t (min) is the contact time; k_1 (min^{-1}) is the rate constant of the pseudo-first-order adsorption; k_2 (g (mg min)$^{-1}$) is the rate constant of the pseudo-second-order adsorption.

The results of pseudo-first-order and pseudo-second-order kinetics for adsorption of Cr(VI) on the Fe–Mn binary oxide absorbent were shown in Fig. 7e and f, respectively. The adsorption rate constants obtained from the adsorption kinetics were listed in Table 3.

As shown in Fig. 7e and f and Table 3, the regression coefficients indicated that the adsorption behavior was better represented by the pseudo-second-order model. The theoretical q_e values are the equilibrium concentrations of Cr(VI) in the adsorbed Fe–Mn binary oxide assuming 90% of Cr(VI) is removed. The calculated q_e values are in agreement with the theoretical ones, and the plots show quite good linearity with R^2 above 0.999. Therefore, the adsorption kinetics follows the pseudo-second-order model, suggesting the rate-limiting step of the adsorption was dominated by a chemical adsorption process.[53]

3.3.3 Adsorption mechanism of Fe–Mn binary oxide adsorbent. As we all know, there are five species (H_2CrO_4, $HCrO_4^-$, CrO_4^{2-}, $HCr_2O_7^-$, and $Cr_2O_7^{2-}$) existing in the Cr(VI) solution are as follows:[56,57]

$$H_2CrO_4 \rightleftharpoons HCrO_4^- + H^+ \quad k_1 = 1.58 \times 10^{-1}$$

$$HCrO_4^- \rightleftharpoons CrO_4^{2-} + H^+ \quad k_2 = 3.16 \times 10^{-7}$$

$$2HCrO_4^- \rightleftharpoons Cr_2O_7^{2-} + H_2O \quad k_3 = 3.31 \times 10$$

$$HCr_2O_7^- \rightleftharpoons Cr_2O_7^{2-} + H^+ \quad k_4 = 1.17$$

With acidic condition (pH < 4.81), –OH was easier to be protonated to form –OH_2^+, hence the electrostatic interaction between –OH_2^+ and Cr-containing anions ($HCrO_4^-$, CrO_4^{2-}, $HCr_2O_7^-$, and $Cr_2O_7^{2-}$) played an essential role in enhancing the

Table 3 Kinetic model parameters for Cr(VI) adsorption on Fe−Mn based adsorbent at absorbent dosage = 0.15 g, temperature = 25 ± 1 °C and pH = 3

C_0 (mg L^{-1})	$q_e*{}^a$ (mg g^{-1})	Pseudo-first-order			Pseudo-second-order		
		k_1	$q_e{}^b$ (mg g^{-1})	R^2	k_2	$q_e{}^b$ (mg g^{-1})	R^2
5	1.53	0.1769	0.47	0.6747	3.2758	1.53	1.0000
50	16.01	0.1596	8.18	0.9403	0.1067	16.15	0.9998
100	30.83	0.1418	9.02	0.8843	0.0915	30.96	0.9999

^{a} The adsorbing capacity on adsorption test. ^{b} The adsorbing capacity on theoretical calculation.
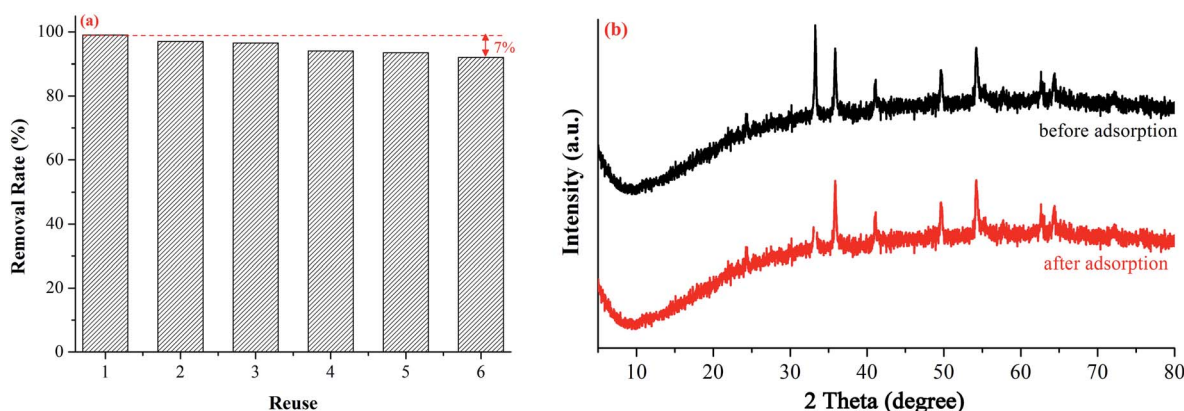
Fig. 8 Adsorption stability (a) and XRD pattern before and after adsorption (b) of Fe−Mn binary oxide adsorbent.

adsorption capacity of Fe–Mn binary oxide adsorbent at pH = 3. The origin of the adsorption ability was the protonation process between H^+ and oxygen-containing functional groups on the surface of Fe–Mn binary oxide, and this reaction process generated some positive charges. Then the positive charges on the surface of Fe–Mn binary oxide had electrostatic adsorption with anions (negative charges). With the pH value increasing (pH > 4.81), the amount of generated positive charges decreased, and the adsorption capacity of Fe–Mn binary oxide was decreased.[58,59]

3.4 Adsorption stability of Fe–Mn binary oxide adsorbent

Some experiments were carried out to confirm the stability of the Fe–Mn binary oxide adsorbent. It has been confirmed that Fe–Mn binary oxide adsorbent shows excellent adsorbing stability with initial molar ratio between Fe and Mn = 3 : 1, adsorbent dosage = 0.15 g, pH value = 3 and initial concentration of Cr(VI) = 20 mg L^{-1} during six cycles, as shown in Fig. 8a. After six rounds of adsorption, the removal rate of Cr(VI) was decreased from 99% to 92% (7% decrease).[60,61]

The XRD patterns and FTIR spectrum of the Fe–Mn binary oxide adsorbent before and after the adsorption reaction are shown in Fig. 8b and 2b. The shape of XRD patterns and FTIR spectrum after the adsorption experiment is similar to those before the reaction, indicating that the structure of the Fe–Mn binary oxide adsorbent does not change during the adsorption process. Hence, the adsorbing stability of Fe–Mn binary oxide adsorbent is dependent on the stability of its structure.[62,63]

4. Conclusions

A novel Fe–Mn binary oxide adsorbent was prepared via a "two-step method" combined with the co-precipitation method and hydrothermal method. The prepared Fe–Mn binary oxide absorbent was characterized by TEM, SEM, XRD, FTIR, TGA, Zeta potential, BET and XPS analysis. The results indicated that the morphology of adsorbent was rod-like with length about 100 nm and width about 50–60 nm, specific surface area was 63.297 m^2 g^{-1}, composition of α-Fe_2O_3 and β-MnO_2 and $MnFe_2O_4$ and the isoelectric point was observed at pH value of 4.81. The removal of Cr(VI) was chosen as a model reaction to evaluate the adsorption capacity of the Fe–Mn binary oxide adsorbent. The adsorption activity was influenced by the molar ratio between Fe and Mn, adsorbent dosage, pH value and initial concentration of Cr(VI) on adsorption of Cr(VI). The adsorption behavior of Fe–Mn binary oxide was better represented by the Freundlich model (adsorption isotherm) and the pseudo-second-order model (adsorption kinetic). The Fe–Mn binary oxide adsorbent showed high adsorption performance and excellent adsorption stability. The possible adsorption mechanism of Fe–Mn binary oxide for the removal of Cr(VI) included the protonation process and the electrostatic attraction interaction.

Conflicts of interest

There are no conflicts to declare.

Acknowledgements

References

1 M. Shahid, S. Shamshad, M. Rafiq, S. Khalid, I. Bibi, N. Niazi, C. Dumat and M. Rashid, Chromium speciation, bioavailability, uptake, toxicity and detoxification in soil-plant system: a review, *Chemosphere*, 2017, **178**, 513–533.

2 Z. Ai, Y. Cheng, L. Zhang and J. Qiu, Efficient removal of Cr(VI) from aqueous solution with Fe@Fe_2O_3 core-shell nanowires, *Environ. Sci. Technol.*, 2008, **42**(18), 6955–6960.

3 C. McClain, S. Fendorf, S. Webb and K. Maher, Quantifying Cr(VI) production and export from serpentine soil of the California coast range, *Environ. Sci. Technol.*, 2016, **51**(1), 141–149.

4 Y. Xing, X. Chen and D. Wang, Electrically regenerated ion exchange for removal and recovery of Cr(VI) from wastewater, *Environ. Sci. Technol.*, 2007, **41**(4), 1439–1443.

5 Y. Liu, H. Li, G. Tan and X. Zhu, Fe^{2+}-modified vermiculite for the removal of chromium(VI) from aqueous solution, *Sep. Sci. Technol.*, 2010, **46**(2), 290–299.

6 M. Gasser, G. Morad and H. Aly, Batch kinetics and thermodynamics of chromium ions removal from waste solutions using synthetic adsorbents, *J. Hazard. Mater.*, 2007, **142**(1–2), 118–129.

7 L. Alidokht, A. Khataee, A. Reyhanitabar and S. Oustan, Reductive removal of Cr(VI) by starch-stabilized Fe^0 nanoparticles in aqueous solution, *Desalination*, 2011, **270**(1–3), 105–110.

8 B. Xie, C. Shan, Z. Xu, X. Li, X. Zhang, J. Chen and B. Pan, One-step removal of Cr(VI) at alkaline pH by UV/sulfite process: reduction to Cr(III) and in situ Cr(III) precipitation, *Chem. Eng. J.*, 2017, **308**, 791–797.

9 L. Li, X. Feng, R. Han, S. Zhang and G. Yang, Cr(VI) removal via anion exchange on a silver-triazolate MOF, *J. Hazard. Mater.*, 2017, **321**, 622–628.

10 S. Koushkbaghi, P. Jafari, J. Rabiei, M. Irani and M. Aliabadi, Fabrication of PET/PAN/GO/Fe_3O_4 nanofibrous membrane for the removal of Pb(II) and Cr(VI) ions, *Chem. Eng. J.*, 2016, **301**, 42–50.

11 Y. Han, X. Cao, X. Ouyang, P. Sohi and J. Chen, Adsorption kinetics of magnetic biochar derived from peanut hull on removal of Cr(VI) from aqueous solution: effects of production conditions and particle size, *Chemosphere*, 2016, **145**, 336–341.

12 Z. Guo, N. Martucci, F. Moreno-Olivas, E. Tako and G. Mahler, Titanium dioxide nanoparticle ingestion alters nutrient absorption in an in vitro model of the small intestine, *Nanoimpact*, 2017, **5**, 70–82.

13 Ihsanullah, A. Abbas, A. Al-Amer, T. Laoui, M. Al-Marri, M. Nasser, M. Khraisheh and M. Atieh, Heavy metal removal from aqueous solution by advanced carbon

nanotubes: critical review of adsorption applications, *Sep. Purif. Technol.*, 2016, **157**, 141–161.

14 Y. Zhang, B. Wu, H. Xu, H. Liu, M. Wang, Y. He and B. Pan, Nanomaterials-enabled water and wastewater treatment, *Nanoimpact*, 2016, **3–4**, 22–39.

15 S. Zhang, H. Zhang, F. Liu, F. Yang, S. Zhou, K. Zheng, C. Chu, L. Liu and M. Ju, Effective removal of Cr(VI) from aqueous solution by biochar supported manganese sulfide, *RSC Adv.*, 2019, **9**(54), 31333–31342.

16 V. Pakade, N. Tavengwa and L. Madikizelac, Recent advances in hexavalent chromium removal from aqueous solutions by adsorptive methods, *RSC Adv.*, 2019, **9**(45), 26142–26164.

17 P. Ghosh, Hexavalent chromium [Cr(VI)] removal by acid modified waste activated carbons, *J. Hazard. Mater.*, 2009, **171**(1–3), 116–122.

18 F. Granados-Correa and S. Bulbulian, Co(II) adsorption in aqueous media by a synthetic Fe-Mn binary oxide adsorbent, *Water, Air, Soil Pollut.*, 2012, **223**(7), 4089–4100.

19 D. Mamais, C. Noutsopoulos, I. Kavallari, E. Nyktari, A. Kaldis, E. Panousi, G. Nikitopoulos, K. Antoniou and M. Nasioka, Biological groundwater treatment for chromium removal at low hexavalent chromium concentrations, *Chemosphere*, 2016, **152**, 238–244.

20 B. Manning, J. Kiser, H. Kwon and S. Kanel, Spectroscopic investigation of Cr(III)- and Cr(VI)-treated nanoscale zerovalent iron, *Environ. Sci. Technol.*, 2007, **41**(2), 586–592.

21 R. Ludwig, C. Su, T. Lee, R. Wilkin, S. Acree, R. Ross and A. Keeley, In situ chemical reduction of Cr(VI) in groundwater using a combination of ferrous sulfate and sodium dithionite: a field investigation, *Environ. Sci. Technol.*, 2007, **41**(15), 5299–5305.

22 J. Zhu, Z. Lou, Y. Liu, R. Fu, S. Baig and X. Xu, Adsorption behavior and removal mechanism of arsenic on graphene modified by iron-manganese binary oxide (FeMnO$_x$/RGO) from aqueous solutions, *RSC Adv.*, 2015, **5**(83), 67951–67961.

23 N. Singh, K. Kezo, A. Debnath and B. Saha, Enhanced adsorption performance of a novel Fe-Mn-Zr metal oxide nanocomposite adsorbent for anionic dyes from binary dye mix: response surface optimization and neural network modeling, *Appl. Organomet. Chem.*, 2018, **32**(3), e4165.

24 J. Hu, M. Irene and G. Chen, Fast removal and recovery of Cr(VI) using surface-modified jacobsite (MnFe$_2$O$_4$) nanoparticles, *Langmuir*, 2005, **21**(24), 11173–11179.

25 E. Deschamps, V. Ciminelli and W. Höll, Removal of As(III) and As(v) from water using a natural Fe and Mn enriched sample, *Water Res.*, 2005, **39**(20), 5212–5220.

26 G. Zhang, J. Qu, H. Liu, R. Liu and R. Wu, Preparation and evaluation of a novel Fe-Mn binary oxide adsorbent for effective arsenite removal, *Water Res.*, 2007, **41**(9), 1921–1928.

27 Z. Lou, Z. Cao, J. Xu, X. Zhou, J. Zhu, X. Liu, S. Baig, J. Zhou and X. Xu, Enhanced removal of As(III)/(v) from water by simultaneously supported and stabilized Fe-Mn binary oxide nanohybrids, *Chem. Eng. J.*, 2017, **322**, 710–721.

28 Q. Ning, Y. Liu, S. Liu, L. Jiang, G. Zeng, Z. Zeng, X. Wang, J. Li and Z. Kare, Fabrication of hydrochar functionalized Fe-Mn binary oxide nanocomposites: characterization and 17β-estradiol removal, *RSC Adv.*, 2017, **7**(59), 37122–37129.

29 W. El-Mehalmey, A. Ibrahim, A. Abugable, M. Hassan, R. Haikal, S. Karakalos, O. Zakid and M. Alkordi, Metal-organic framework@silica as a stationary phase sorbent for rapid and cost-effective removal of hexavalent chromium, *J. Mater. Chem. A*, 2018, **6**(6), 2742–2751.

30 S. Zhu, X. Huang, D. Wang, L. Wang and F. Ma, Enhanced hexavalent chromium removal performance and stabilization by magnetic iron nanoparticles assisted biochar in aqueous solution: mechanisms and application potential, *Chemosphere*, 2018, **207**, 50–59.

31 X. Zhang, J. Dong, Z. Hao, W. Cai and F. Wang, Fe-Mn/MCM-41: Preparation, characterization, and catalytic activity for methyl orange in the process of heterogeneous Fenton reaction, *Trans. Tianjin Univ.*, 2018, **24**(4), 361–369.

32 Z. Yuan, X. Cheng, L. Zhong, R. Wu and Y. Zheng, Preparation, characterization and performance of an electrospun carbon nanofiber mat applied in hexavalent chromium removal from aqueous solution, *J. Environ. Sci.*, 2019, **77**, 75–84.

33 C. Kim, C. Lee, Y. Song, J. Heo, S. Choi, D. Lim, J. Cho, C. Park, M. Jang and J. Kim, Hexavalent chromium as a cathodic electron acceptor in a bipolar membrane microbial fuel cell with the simultaneous treatment of electroplating wastewater, *Chem. Eng. J.*, 2017, **328**(15), 703–707.

34 G. Zhu, J. Song, W. Dong, J. Lu, Y. Wang, W. Jiang and P. Guo, Removal of hexavalent chromium from water by modified sponge iron particles and insights into mechanism, *Environ. Sci. Pollut. Res.*, 2018, **25**(26), 26173–26181.

35 J. Yu, H. Wang and Q. Ji, Investigating adsorption mechanism and surface complex formation modeling for aqueous sulfadiazine bonding on Fe/Mn binary oxides, *Environ. Sci. Pollut. Res.*, 2019, **26**(22), 23162–23172.

36 Y. Song, L. He, X. Chen and Z. Zhao, Removal of tungsten from molybdate solution by Fe-Mn binary oxide adsorbent, *Trans. Nonferrous Met. Soc. China*, 2017, **27**(11), 2492–2502.

37 A. Asfaram, M. Ghaedi, S. Hajati, A. Goudarzi and E. Dil, Screening and optimization of highly effective ultrasound-assisted simultaneous adsorption of cationic dyes onto Mn-doped Fe$_3$O$_4$-nanoparticle-loaded activated carbon, *Ultrason. Sonochem.*, 2017, **34**, 1–12.

38 M. Szumera and B. Łagowska, Spectroscopic studies of MnO$_2$ and SiO$_2$ containing soil-active phosphate glasses, *J. Appl. Spectrosc.*, 2017, **83**(6), 951–958.

39 M. Szlachta and N. Chubar, The application of Fe-Mn hydrous oxides based adsorbent for removing selenium species from water, *Chem. Eng. J.*, 2013, **217**, 159–168.

40 L. Zhang, X. Liu, X. Huang, W. Wang, P. Sun and Y. Li, Adsorption of Pb^{2+} from aqueous solutions using Fe-Mn binary oxides-loaded biochar: kinetics, isotherm and thermodynamic studies, *Environ. Technol.*, 2019, **40**(14), 1853–1861.

41 L. Jiang, Y. Gu, H. Guo, L. Liu and J. Chen, Efficient removal of 17α-ethinylestradiol (EE2) from water using freshly

formed Fe-Mn binary oxide, *RSC Adv.*, 2017, **7**(38), 23802–23811.

42 B. Ensano, M. Luna, K. Rivera, S. Pingul-Ong and D. Ong, Optimization, isotherm, and kinetic studies of diclofenac removal from aqueous solutions by Fe-Mn binary oxide adsorbents, *Environ. Sci. Pollut. Res.*, 2019, **26**(31), 32407–32419.

43 G. Zhang, H. Liu, R. Liu and J. Qu, Removal of phosphate from water by a Fe-Mn binary oxide adsorbent, *J. Colloid Interface Sci.*, 2009, **335**(2), 168–174.

44 J. Das, D. Das, G. Dash and K. Parida, Studies on Mg/Fe hydrotalcite-like-compound (HTlc): I. Removal of inorganic selenite (SeO_3^{2-}) from aqueous medium, *J. Colloid Interface Sci.*, 2002, **251**(1), 26–32.

45 M. Jang, S. Min, T. Kim and J. Park, Removal of arsenite and arsenate using hydrous ferric oxide incorporated into naturally occurring porous diatomite, *Environ. Sci. Technol.*, 2006, **40**(5), 1636–1643.

46 M. Toor and B. Jin, Adsorption characteristics, isotherm, kinetics, and diffusion of modified natural bentonite for removing diazo dye, *Chem. Eng. J.*, 2012, **187**, 79–88.

47 X. Deng, L. Qi and Y. Zhang, Experimental study on adsorption of hexavalent chromium with microwave-assisted alkali modified fly ash, *Water, Air, Soil Pollut.*, 2018, **229**(1), 18.

48 B. Yousaf, G. Liu, Q. Abbas, R. Wang, H. Ullah, M. Mian, A. Yousaf and A. Rashid, Enhanced removal of hexavalent chromium from aqueous media using a highly stable and magnetically separable rosin-biochar-coated TiO_2@C nanocomposite, *RSC Adv.*, 2018, **8**(46), 25983–25996.

49 C. Lee and Y. Bae, Effect of surfactants on the swelling behaviors of thermosensitive hydrogels: applicability of the generalized Langmuir isotherm, *RSC Adv.*, 2016, **6**(105), 103811–103821.

50 P. Borys and Z. Grzywna, On the fractality of the Freundlich adsorption isotherm in equilibrium and non-equilibrium cases, *Phys. Chem. Chem. Phys.*, 2016, **18**(30), 20784–20789.

51 H. Hu, Y. Gao, T. Wang, L. Sun, Y. Zhang and H. Li, Removal of hexavalent chromium, an analogue of pertechnetate, from aqueous solution using bamboo (Acidosasa edulis) shoot shell, *J. Radioanal. Nucl. Chem.*, 2019, **321**(2), 427–437.

52 A. Bhattacharya, T. Naiya, S. Mandal and S. Das, Adsorption, kinetics and equilibrium studies on removal of Cr(VI) from aqueous solutions using different low-cost adsorbents, *Chem. Eng. J.*, 2008, **137**(3), 529–541.

53 H. Jin, Z. Ji, J. Yuan, J. Li, M. Liu, C. Xu, J. Dong, P. Hou and S. Hou, Research on removal of fluoride in aqueous solution by alumina-modified expanded graphite composite, *J. Alloys Compd.*, 2015, **620**, 361–367.

54 O. Moradi, A. Fakhri, S. Adami and S. Adami, Isotherm, thermodynamic, kinetics, and adsorption mechanism studies of ethidium bromide by single-walled carbon nanotube and carboxylate group functionalized single-walled carbon nanotube, *J. Colloid Interface Sci.*, 2013, **395**, 224–229.

55 M. Alikhani and M. Moghbeli, Ion-exchange polyHIPE type membrane for removing nitrate ions: preparation, characterization, kinetics and adsorption studies, *Chem. Eng. J.*, 2014, **239**, 93–104.

56 G. Zhang, H. Liu, R. Liu and J. Qu, Adsorption behavior and mechanism of arsenate at Fe-Mn binary oxide/water interface, *J. Hazard. Mater.*, 2009, **168**(2–3), 820–825.

57 H. Shen, S. Pan, Y. Zhang, X. Huang and H. Gong, A new insight on the adsorption mechanism of amino-functionalized nano-Fe_3O_4 magnetic polymers in Cu(II), Cr(VI) co-existing water system, *Chem. Eng. J.*, 2012, **183**, 180–191.

58 Z. Yan, Y. Liu, X. Tan, S. Liu, G. Zeng, L. Jiang, M. Li, Z. Zhou, S. Liu and X. Cai, Immobilization of aqueous and sediment-sorbed ciprofloxacin by stabilized Fe-Mn binary oxide nanoparticles: influencing factors and reaction mechanisms, *Chem. Eng. J.*, 2017, **314**, 612–621.

59 K. Lu, T. Wang, L. Zhai, W. Wu, S. Dong, S. Gao and L. Mao, Adsorption behavior and mechanism of Fe-Mn binary oxide nanoparticles: adsorption of methylene blue, *J. Colloid Interface Sci.*, 2019, **539**, 553–562.

60 N. Lotlikar, S. Damare, R. Meena, P. Linsy and B. Mascarenhas, Potential of marine-derived fungi to remove hexavalent chromium pollutant from culture broth, *Indian J. Microbiol.*, 2018, **58**(2), 182–192.

61 R. Mokkapati, V. Ratnakaram and J. Mokkapati, Utilization of agro-waste for removal of toxic hexavalent chromium: surface interaction and mass transfer studies, *Int. J. Environ. Sci. Technol.*, 2018, **15**(4), 875–886.

62 S. Ryu, E. Jeon, J. Yang and K. Baek, Adsorption of As(III) and As(V) in groundwater by Fe-Mn binary oxide-impregnated granular activated carbon (IMIGAC), *J. Taiwan Inst. Chem. Eng.*, 2017, **72**, 62–69.

63 C. McCann, C. Peacock, K. Hudson-Edwards, T. Shrimpton, N. Gray and K. Johnson, In situ arsenic oxidation and sorption by a Fe-Mn binary oxide waste in soil, *J. Hazard. Mater.*, 2018, **342**, 724–731.